TITLE: Genetic context drives age-related disparities in synaptic maintenance and structure across cortical and hippocampal neuronal circuits.

Sarah E. Heuer[1,2], Emily W. Nickerson[1,2], Gareth R. Howell[1,2,3,*], Erik B. Bloss[1,2,3,*]

[1]The Jackson Laboratory, Bar Harbor, ME 04609, USA

[2]Tufts University Graduate School of Biomedical Sciences, Boston, MA 02111, USA

[3]Graduate School of Biomedical Sciences and Engineering, University of Maine, Orono, Maine 04469, USA

[*]Correspondence: erik.bloss@jax.org, gareth.howell@jax.org

KEYWORDS

Aging, dendritic spines, frontal cortex, neuronal circuits, genetic diversity

ABSTRACT

The disconnection of neuronal circuits through synaptic loss is presumed to be a major driver of age-related cognitive decline. Age-related cognitive decline is heterogeneous, yet whether genetic mechanisms differentiate successful from unsuccessful cognitive decline through synaptic structural mechanisms remains unknown. Previous work using rodent and primate models leveraged various techniques to suggest that age-related synaptic loss is widespread on pyramidal cells in prefrontal cortex (PFC) circuits but absent on those in area CA1 of the hippocampus. Here, we examined the effect of aging on synapses on projection neurons forming a hippocampal-cortico-thalamic circuit important for spatial working memory tasks from two genetically distinct mouse strains that exhibit susceptibility (C57BL/6J) or resistance (PWK/PhJ) to cognitive decline during aging. Across both strains, synapses on the CA1-to-PFC projection neurons appeared completely intact with age. In contrast, we found synapse loss on PFC-to-nucleus reuniens (RE) projection neurons from aged C57BL/6J but not PWK/PhJ mice. Moreover, synapses from aged PWK/PhJ mice but not from C57BL/6J exhibited morphological changes that suggest increased synaptic efficiency to depolarize the parent dendrite. Our findings suggest resistance to age-related cognitive decline results in part by age-related synaptic adaptations, and identification of these mechanisms in PWK/PhJ mice could uncover new therapeutic targets for promoting successful cognitive aging and extending human health span.

53 **INTRODUCTION**

54 Synapses are the fundamental computational subunits of the brain, and the building blocks
55 of neuronal circuits that vary in complexity based on brain region and mammalian organism (1,
56 2). Synapses enable cell-type specific forms of communication and are often targeted to defined
57 spatial subcellular locations on postsynaptic cell types (3), which constrains neural circuit
58 operations (4, 5). Synapses act as plastic, tunable biochemical and electrical signaling
59 compartments, a feature that allows internal states to shape neural circuit function (6, 7), and may
60 be the primary substrate in the nervous system mediating learning and memory recall (8, 9).

61 Individual excitatory synapses on many neuronal cell types take the form of small
62 protrusions along the dendrites (i.e., dendritic spines (10)), which can be visualized by multiple
63 imaging methods (8, 11, 12). Spine structure reflects the functional strength of each connection:
64 spine head size correlates with synapse strength (8, 12), and the morphology of the spine neck
65 determines the degree of electrical and biochemical filtering that occurs between the synapse and
66 the parent dendritic cable (13, 14). During normal aging, mammalian organisms experience
67 progressive, yet variable, cognitive decline, even in the absence of a disease, which corresponds
68 to a loss in synaptic plasticity(15). Relative to other synapses, spine synapses seem to be the
69 primary type that are lost or altered during aging, and these changes in the aging brain appear
70 circuit specific (16, 17). For example, the density of spine synapses decrease over time on cortical
71 neurons in the frontal but not visual cortex, and decrease on CA3 pyramidal neurons but not on
72 neighboring neurons in CA1 (16, 18, 19). The loss of synapse number and the changes in synaptic
73 structure on frontal cortical neurons correlate with progressive decreases in cognitive function
74 with age (20–22), yet reports of the degree to which synaptic loss occurs suggests significant
75 heterogeneity (16, 23–25). The causal factors that underlie this variability could be what
76 determines successful versus unsuccessful neural aging (16, 26, 27), and there is significant
77 interest in understanding how genetic components and environmental influences coordinately
78 shape the trajectory of age-related cognitive changes and synaptic connectivity.

79 Non-human primates (NHPs) (22, 28, 29) and rodents (rats (25, 30, 31) and mice (32))
80 are commonly used model systems to study the effect of aging on synapses. Although NHPs are
81 the most translatable model for relating age-related neural circuit changes to cognitive decline
82 (22, 33), they have long lifespans (>30 years), require complex housing systems, and are not
83 amendable to genetic-based experimentation at scale. However, to a large extent, data from
84 rodent models recapitulate the magnitude of age-related synaptic loss in vulnerable brain regions
85 (including the prefrontal cortex) that has been observed in NHPs (24, 25, 34). Studies in mice
86 have shown loss in synaptic plasticity and number during aging and in age-related diseases (35,
87 36). Unlike NHP experiments, which necessarily use genetically diverse non-inbred subjects, the
88 work in mice has largely been performed using the inbred C57BL/6J (B6) mouse strain. The lack
89 of genetic diversity limits translatability of mouse work to humans, and led us to evaluate the
90 potential of incorporating genetically distinct wild-derived inbred mouse strains in our own work
91 (37). Our previous results show wild-derived strains exhibit diverse cognitive and behavioral
92 phenotypes during aging and when carrying Alzheimer's disease (AD)-linked transgenes,
93 suggesting genetic background strongly influences neuronal circuitry and function (38, 39). In
94 particular, the PWK/PhJ (PWK) mouse strain did not show amyloid-dependent cognitive decline
95 or synaptic loss, suggesting PWK is an ideal strain to study resilience to AD (40). However, the
96 neuronal circuits vulnerable in aging are different than those vulnerable to AD, and it remains
97 unknown whether PWK is also resistant to normal age-related synaptic loss.

98 To determine the effect of genetic context on age-related synapse dynamics (and how
99 they might relate to their observed cognitive susceptibility/resilience (38, 41)), we examined aging-
100 related synapse loss in the traditionally studied B6 mouse strain and the wild-derived PWK. PWK
101 mice differ from B6 by approximately 20 million single nucleotide polymorphisms (SNPs) and
102 structural variants (37). To target our analyses to specific projection neurons, we leveraged
103 retrograde viral strategies to label two circuits known to have different vulnerabilities to aging or
104 AD: PFC-projecting neurons to nucleus reuniens (RE; PFC-to-RE), and CA1-projecting neurons

105 to PFC (CA1-to-PFC) (17). Spine synapses on CA1-to-PFC neurons showed marked stability
106 throughout aging in both B6 and PWK mice. In contrast, PFC-to-RE neurons were susceptible to
107 age-related spine loss in B6 but not PWK. Further, there were morphological changes suggestive
108 of synapse strengthening in PWK but not B6 mice. Collectively, these results provide evidence
109 that PWK are a model of successful synaptic aging.
110

111 **RESULTS**

112 **Labeling strategies to visualize synapses from two neural circuits in genetically distinct**
113 **mice.**

114 Our previous studies suggest PWK are a model of cognitive, neuronal and synaptic
115 resilience to Aβ pathology (38, 40). However, since age is the leading risk factor for developing
116 AD, we tested the prediction that PWK would also be a model of successful synaptic aging when
117 compared to traditionally used inbred B6 mice. We leveraged previously established viral
118 approaches (42, 43) using two different fluorophores to label excitatory projection neurons forming
119 two arms of a connected hippocampal-cortico-thalamic loop important for spatial working memory
120 tasks (44). Each set of projection neurons expressed either EGFP or tdTomato across cohorts of
121 female B6 and PWK mice ranging from 4-29 months of age (see **Table S1**). Three unilateral
122 intracranial injection sites were targeted to deliver recombinant adenoassociated virus (AAV, see
123 **Methods**) to drive EGFP in PFC neurons that project to RE (PFC-to-RE) and tdTomato
124 expression in CA1 neurons that project to PFC (CA1-to-PFC). After allowing 3-4 weeks for proper
125 retrograde movement and fluorophore expression each mouse was perfused, coronal slices were
126 made with a vibratome, slices containing EGFP+ or tdTomato+ neurons were imaged, and
127 dendritic spine density and morphologies were analyzed (**Figure 1A**). Three age groups were
128 assessed: young (4-7 months of age), middle-aged (11-17 months of age) and aged (22-30
129 months of age) groups. Neurons making up the two projection circuits in B6 and PWK mice were

130 labeled with equivalent efficiency, suggesting a similar overall density of neurons comprising
131 these pathways from the compared strains (**Figure 1B-C**).
132
133 **Aging spines on proximal CA1 dendrites exhibit stable densities but altered morphologies**
134 **in PWK but not B6 mice**
135 The CA1 region of the hippocampus is well-studied on account of its anatomy, physiology,
136 role in episodic memory, and vulnerability to both age- and AD-related pathological insults (27).
137 While generally thought to be relatively resistant to normal age-related synaptic loss (45–47), it is
138 unclear if age-related structural changes occur on specific CA1 projections, and if they are
139 modulated in subjects from genetic contexts that exhibit resistance to cognitive aging. The
140 majority of excitatory inputs onto CA1 pyramidal cells are made onto the proximal apical oblique
141 and basal branches (48, 49) which both receive inputs from hippocampal area CA3 (50).
142 Therefore, we first analyzed dendritic spine synapses on branches from this proximal
143 compartment specifically on CA1-to-PFC neurons (**Figure 2A**). Consistent with the prediction
144 from previous reports (17, 45), we observed no significant age-related changes in proximal spine
145 density in either B6 or PWK mice (**Figure 2B-C**).
146 Dendritic spines alter their morphologies in response to repeated artificial synaptic
147 stimulation (6, 9), under conditions of homeostasis (7, 51), and in reaction to disease pathologies
148 and during aging (52, 53). Spine head morphology is a reliable predictor of synaptic stability and
149 strength (8, 12), so we analyzed the maximum head diameter of each reconstructed spine. Our
150 analysis found no overt age-related changes in B6 mice, but the same analysis in PWK mice
151 revealed a subtle yet significant age-related shift to spines with smaller head diameters (**Figure**
152 **2D**). This effect was evident when we examined the densities of spines across the smallest (Q1)
153 and largest (Q4) quartiles of head diameters (**Figure S1B**).
154 The morphology of dendritic spine necks (e.g. neck width and length) are similarly plastic
155 (13) and define the compartmentalization of spines much more critically than spine head size (13,

156 14, 54, 55). Dendritic spine necks act as strong electrical resistors, filtering currents from the
157 synapse to the parent dendrite branch (54). Necks also contain receptors for neuromodulatory
158 systems that regulate local excitability (56). Spine necks are often below 50 nm (49) making them
159 hard to resolve with light microscopy techniques, thus we analyzed putative spine neck lengths
160 to determine whether this aspect of spine neck morphology is readily modified during aging. Neck
161 lengths in B6 mice were slightly lengthened with age, complementing the stability observed in
162 spine heads. In contrast, PWK spine neck lengths showed a biphasic response, first increasing
163 from young to middle-aged, then decreasing significantly in aged mice compared to the younger
164 groups (**Figure 2E**, **Figure S1C**).
165
166 **Spine changes on distal CA1 dendrites mirror those found on proximal compartments**
167 Distal tuft dendrites in CA1 pyramidal cells are thought to be the most vulnerable to AD-
168 related synaptic changes due to their afferent inputs originating in the EC (**Figure 3A**) (57), where
169 associated neuropathology is observed very early in the disease process (58, 59). Synapses on
170 distal dendrites are understudied relative to those on more proximal compartments due to
171 limitations in traditional techniques used to evaluate plasticity at remote locations relative to the
172 soma. Consistent with our results from the proximal dendrites, we observed no significant age-
173 related changes to distal tuft spine densities in B6 or PWK mice (**Figure 3B-C**). Like spines from
174 proximal branches, we observed few age-related changes in head diameter and neck length in
175 spines from B6 distal branches (**Figure 3D-E, Figure S2B-C**). However, spine head diameters
176 were larger in aged PWK mice compared to young and middle-aged cohorts (**Figure 3D**, **Figure**
177 **S2B**), and spine neck lengths were significantly shorter in aged compared to young and middle-
178 aged mice (**Figure 3E**, **Figure S2C**).
179 Collectively, these results show spine densities on proximal and distal dendrites from CA1-
180 to-PFC pyramidal cells do not change with age in both B6 and PWK mice. Furthermore, B6 spines
181 remained morphologically stable whereas PWK spines exhibited changes indicative of increased

182 excitability at the synapse and to the parent dendritic cable, which support the notion that these
183 adaptations could play a role in maintaining information processing in the aging hippocampus.
184
185 **Differential vulnerability to age-related synaptic changes on PFC-to-RE neurons across B6**
186 **and PWK mice**
187 Previous studies in humans, NHPs, rats and mice report that pyramidal neurons in the
188 prefrontal cortex are susceptible to synaptic loss with age (21, 22, 25, 29, 60). Moreover,
189 preventing this degeneration could be key to promoting successful cognitive aging (21, 61, 62).
190 To test the prediction that PWK mice are resistant to age-dependent synaptic loss in the PFC, we
191 used AAVs to also label deep-layer neurons (in the exact mice described above) in the PFC that
192 project to the RE (**Figure 1**) that appear to mediate behavioral flexibility and working memory
193 (63–65). Like the CA1-to-PFC neurons, PFC-to-RE neurons have a similar proximal-distal
194 dendritic architecture, and each compartment receives a distinct set of inputs. Basal and apical
195 oblique dendrites located in the proximal regions receive afferent inputs from CA1 (among other
196 regions), whereas distal tuft receive a distinct set of inputs from the thalamus (43) (**Figure 4A**).
197 Therefore, we analyzed the spines on proximal and distal dendrites separately.
198 We first examined spine density on proximal dendrites of PFC-to-RE neurons. Consistent
199 with previous findings, B6 proximal dendritic spine density was significantly lower in middle-aged
200 and aged compared to young mice (66). Interestingly, we found no differences in spine densities
201 on proximal PFC dendrites across age cohorts in PWK mice (**Figure 4B-C**). When we examined
202 spine morphologies, we found statistically significant changes in spine head diameter with age on
203 both B6 and PWK proximal PFC dendrites, evidenced by the cumulative frequency analyses and
204 by quartile analysis of the largest and smallest spines (**Figure 4D**, **Figure S3B**). In both B6 and
205 PWK mice, PFC proximal spine head diameters became subtly larger with aging (**Figure 4D**).
206 Interestingly, spines on proximal dendrites from B6 mice showed minimal age-related changes in
207 spine neck length. However, spines on proximal branches from PWK mice were significantly

208 shortened with age, changes that should reduce neck-related filtering of synaptic currents,
209 mimicking the same patterns found on aging CA1 dendrites from PWK mice (**Figure 4E**, **Figure**
210 **S3C**).
211

212 **Age-related dendritic spine loss and morphological remodeling on distal PFC dendrites**
213 **differs between B6 and PWK mice**

214 Distal tuft branches from PFC-to-RE projection neurons receive distinct afferent inputs
215 compared to proximal branches, coming from the thalamus instead of CA1 (43) (**Figure 5A**).
216 Similar to the age-related changes found on proximal dendrites of PFC-to-RE neurons, distal
217 dendritic spine densities were lower in middle-aged and aged compared to young B6 mice but did
218 not change across age groups in PWK mice (**Figure 5B-C**).

219 Spine head diameters on distal branches of PFC-to-RE neurons from B6 mice showed a
220 biphasic response, first increasing in size between young and middle-aged cohorts, then
221 decreasing in size between middle-aged to aged groups. PWK distal PFC spine heads displayed
222 the opposite pattern: decreasing in size between young and middle-aged groups, and then
223 increasing in size between middle-aged and aged cohorts (**Figure 5D, Figure S4B**). Spine neck
224 lengths on the distal dendrites of PFC-to-RE neurons from B6 mice slightly lengthened with age,
225 while those from PWK decreased more dramatically with age (**Figure 5E**). These changes in
226 spine neck lengths were observed in quartile analyses, with a significant gain of long spine necks
227 in aged B6 mice, and an overt loss of long spine necks in aged PWK mice (**Figure S4C**). These
228 results from distal PFC-to-RE dendrites mirrored those from proximal dendrites: B6 branches
229 showed age-related synaptic loss while those from PWK did not. In contrast, PWK distal PFC
230 spines showed spine neck remodeling while those from B6 were markedly more stable.

231 Collectively, these data support our hypothesis that, like resilience to AD-related Aβ
232 pathology (38), PWK mice show resistance to age-related cortical synapse loss. This resistance
233 was evident across both proximal and distal compartments and accompanied by specific forms

234 of spine head and neck remodeling. Decreases in spine neck length should serve to lower the
235 spine neck resistor and effectively increase the efficiency by which current generated at the
236 synapse reaches the parent dendrite. Given the growing links between dendritic mechanisms of
237 integration and the plasticity that mediates learning and memory (67–70), the putative adaptive
238 spine responses could serve as mechanisms to promote successful maintenance of neuronal
239 health and cognition during aging.
240

241 **DISCUSSION**

242 Here, we asked whether the effects of aging on synapse number and structure in two
243 specific neural circuits was equivalent across two distinct strains of mice. We chose to investigate
244 B6 and PWK strains as our past work has identified them as susceptible or resilient to AD-related
245 cognitive and synaptic deficits, respectively (38, 40, 41). To rigorously compare across defined
246 neural circuits, we used multisite viral injections to label CA1-to-PFC and PFC-to-RE neurons and
247 systematically sampled ~90,000 spines in proximal and distal dendritic compartments across
248 multiple ages (ranging from 5-30 months of age). We found that PFC-projecting CA1 pyramidal
249 cells from both strains maintain their dendritic spine synaptic densities with age, consistent with
250 a body of work examining randomly labeled neurons or synapses in aging NHPs, rats and B6
251 mice (16, 18, 27, 28, 45). Conversely, we observed a differential pattern of synapse loss on RE-
252 projecting PFC neurons between B6 and PWK mice, with synapse loss restricted to B6 but not
253 PWK mice. Spine reconstructions suggested that spines from B6 showed either stability or
254 patterns of remodeling putatively associated with decreased synaptic efficacy, whereas PWK
255 spines tended to show morphological changes consistent with increased synaptic efficacy during
256 aging (**Table S6**). These results suggest that previously observed cognitive characteristics from
257 these strains (38), including PWK resistance to aging-related decline in cognition or resilience to
258 AD-related neuropathology (38) and differential microglia activation (71) may be due in part to an
259 adaptive forms of synaptic plasticity that maintain connectivity and excitability in cortical circuitry.

260 The PWK mouse strain, then, represents an opportunity to identify and harness adaptive
261 mechanisms to lengthen cognitive resistance to the normal process of aging.

262 The high-resolution spine reconstructions performed here and viral-based strategies
263 allowed for specific populations of projection neurons to be compared across mice (42). Past work
264 has relied on disparate techniques, including strategies to label random neurons with dye-filling
265 methods or counting random synapses by EM, to build a coherent picture of synaptic vulnerability
266 of the aging brain (22, 25, 29, 35). By taking advantage of multisite viral strategies to gain
267 projection neuron specificity within the same aging subjects, our results are the beginning of
268 identifying the neural circuits that are vulnerable to age-related disconnection in terms of
269 information flow. Interplay between CA1 of the hippocampus, PFC and RE is thought to be critical
270 for spatial working memory tasks, a cognitive domain affected in aged individuals (44, 65, 72).
271 Since our most striking finding is the strain-dependent loss on aging PFC-to-RE neurons, our
272 results suggest the PFC may be the critical locus of aging in terms of synapse loss. Reductions
273 in PFC-to-RE spine densities in B6 mice was most dramatic from young to middle-aged, which is
274 consistent with previous findings of synapses on PFC neurons from rats (25, 30), as well as with
275 behavioral findings that animals and humans start to become impaired in working memory
276 function tasks as early as middle-age (31, 65, 73, 74). Although CA1 projection neurons appear
277 to maintain their numbers during aging, our results do not imply that CA1 function is intact during
278 aging. Other processes, including activity-dependent spine plasticity at CA1 synapses, might also
279 contribute to age-related deficits in hippocampal-dependent learning or memory function.

280 At the level of individual synapses, spine structure is a strong determinant of function (8,
281 12, 13). Specifically, spine head diameter is a correlate of synapse strength, and spine neck of
282 the level of compartmentalization between the synapse and parent dendrite. Past work has
283 focused on age-related modification of head diameter with little evidence for modulation of spine
284 neck morphology (62). In contrast, our data suggest that both spine head diameter and neck
285 length are readily modified during aging in a way that depends on genetic context. In B6 mice,

286 CA1-to-PFC neurons exhibited very few morphological spine changes with age, consistent with a
287 remarkable population stability during aging. Conversely, PWK mice showed consistent evidence
288 for morphological spine remodeling on CA1-to-PFC and PFC-to-RE neurons that are suggestive
289 of an overall increase in efficacy between the spine synapse and parent dendrite (**Table S6**).
290 These data are compelling because both spine head and spine neck changes move in unison
291 towards greater synapse efficiency, and their synergism might potentially drive large changes in
292 how excitatory postsynaptic potentials from multiple synapses are integrated in the dendrites.
293 Recent work from our group has found that PWK mice are resilient to AD-related synaptic
294 changes in CA1-to-PFC neurons during early exponential phases of pathology spread (40). As
295 biological age is the primary risk factor for developing neurodegenerative disorders including AD
296 (75, 76), the data presented here suggest that the PWK mouse strain can be both a model of
297 resilience to cognitive and synaptic changes seen in AD (38, 40), and resistance to cortical
298 synapse loss seen during normal brain aging. Since the molecular and cellular mechanisms that
299 differentiate successful from unsuccessful agers are still unknown (27), the findings here could
300 drive the identification of cell-specific processes that maintain synapses throughout aging. Future
301 work should seek to advance this goal by testing additional PFC projection neurons to understand
302 the circuit specificity of resistance, by molecular strategies to uncover the gene(s) required for this
303 resistance, and by using functional studies that interrogate how behavior relates to pattens of
304 neuronal activity in these circuits (64, 77). Ultimately, such work would set the stage for developing
305 precise therapeutic strategies to promote healthy cognitive aging and resilience to AD across our
306 genetically diverse and aging human population.
307

308 **MATERIALS AND METHODS**

309 **Ethics Statement**

310 All research was approved by the Institutional Animal Care and Use Committee (IACUC) at The
311 Jackson Laboratory (approval number 12005 and 20006). Animals were humanely euthanized

312 with 4% tribromoethanol (800 mg/kg). Authors performed their work following guidelines
313 established by "The Eight Edition of the Guide for the Care and Use of Laboratory Animals" and
314 euthanasia using methods approved by the American Veterinary Medical Association.
315
316 **Animal husbandry**
317 All mice were bred and housed in a 12/12 hour light/dark cycle on aspen bedding and fed a
318 standard 6% Purina 5K52 Chow diet. Experiments were performed using two mouse strains:
319 C57BL/6J (B6, JAX stock #000664) and PWK/PhJ (PWK, JAX stock #003715). Mice were group
320 housed for entirety of experiments. Experimental cohorts were generated through intercrossing
321 B6 or PWK mice to produce 3-8 female mice per age group. Full mouse information is reported
322 in **Table S1**.
323
324 **Intracranial viral injections**
325 Recombinant adenoassociated viral (AAV) vectors were used to drive Cre-recombinase
326 (AAVretro-Cre)(42), Cre-dependent EGFP (serotype 2/1, AAV-FLEX-*rev*-EGFP) (42, 43), Flp-
327 recombinase (AAVretro-CAG-FLPo), and FLP-dependent tdTomato (serotype 2/1 AAV-CAG-
328 FRT-*rev*-TdTomato) (78). AAVretro-CAG-FLPo and AAV-CAG-FRT-*rev*-TdTomato were gifts
329 from Janelia Viral Tools (Addgene plasmid #183412, http://n2t.net/addgene:183412,
330 RRID:Addgene_183412; Addgene plasmid #191203, http://n2t.net/addgene:191203,
331 RRID:Addgene_191203). The titers of each virus were as follows (in genomic copies/mL):
332 AAVretro-Cre, $1x10^{12}$, AAV-FLEX-*rev*-GFP, $1x10^{13}$, AAVretro-CAG-FLPo, $1x10^{13}$; AAV-CAG-
333 FRT-*rev*-TdTomato, $1x10^{13}$. A 1:1 ratio of AAVretro-CAG-FLPo and AAV-FLEX-*rev*-GFP was
334 mixed and 45nL injected into ventral prefrontal cortex (PFC) over 5 minutes; 45-50 nL (per each
335 D/V coordinate) of AAV-CAG-FRT-*rev*-TdTomato was injected in CA1 (CA1) over 10 minutes;
336 AAVretro-Cre was diluted 1:10 with sterile saline and 45 nL injected into nucleus reunions (RE)
337 over 5 minutes. Since PWK brain volumes are smaller than B6, injection coordinates were

338 adjusted based on pilot experiments to determine injection sites. The coordinates for each
339 injection were as follows (in mm: posterior relative to bregma, lateral relative to midline, and
340 ventral relative to pial surface): B6 PFC (+1.75, -0.95, and -2.6), B6 CA1 (-3.5, -3.4, and -2.7/-
341 2.5/2.0), B6 RE(-1.1, -1.2, -4.15); PWK PFC (+1.45, -0.9, and -2.3), PWK CA1 (-3.5, -3.3, and -
342 2.75/-2.5/-2.0), PWK RE(-1.0, -1.0, -3.2). RE and PFC injections were performed with the mouse
343 tilted at a 15° angle. At each site the injection pipette was left in place for 3-5 minutes then slowly
344 retracted at a rate of 10 μm/s from the brain. After surgery mice were singly housed, monitored
345 for 5 days, and euthanized approximately 3-4 weeks post injection.
346
347 **Tissue harvest and brain sectioning**
348 Mice were euthanized with an intraperitoneal lethal dose of Tribromoethanol (800 mg/kg),
349 followed by transcardial perfusion with 45 mL ice-cold 4% paraformaldehyde (PFA) in 0.1M
350 phosphate-buffered saline, in accordance with IACUC protocols (12005 and 20008). Brains were
351 removed and placed in 5mL ice cold 4% PFA at 4°C for 24 hours, then placed into storage buffer
352 (1XPBS + 0.1% Sodium Azide) for long-term storage at 4°C. Brains were coronally sectioned at
353 50μm thickness and placed in storage buffer at 4°C until needed for imaging. Approximately 6
354 frontal PFC sections containing EGFP+ dendrites, and 6 sections with distal CA1 TdTomato+
355 dendrites were mounted on slides and coverslipped using Vectashield Hardset mounting media
356 (Vector Laboratories #H140010).
357
358 **Dendritic spine imaging and analysis**
359 Slices were imaged on an SP8 confocal microscope equipped with a 63X objective (oil
360 immersion), images collected at 50 nm pixel sizes with 0.1 μm z-steps, and stacks deconvolved
361 using Leica Lightning software. 10 dendrites per compartment (e.g. basal, apical oblique, tuft)
362 were captured per mouse. Each image was exported as TIFF format (in ImageJ version

363 2.9.0/1.53t) and imported into NeuronStudio (79) for analysis of dendritic spine densities and
364 morphologies. Since the effectiveness of a synaptic input on the dendritic tree is influenced by
365 the diameter of the parent dendrite (80), we ensured all dendritic calibers incorporated into this
366 analysis were thin (i.e. under 1 μm in diameter) (**Figure S1A, S2A, S3A, S4A**). Density
367 measurements were acquired by first reconstructing the dendritic cable followed by semi-
368 automated spine identification. Cumulative distributions of assigned spine head diameters
369 (HEAD.DIAMETER) and neck lengths (MAX.DTS) were analyzed by Kolmogorov-Smirnov tests,
370 and through a quartile-based analysis. In this latter analysis, spines within dendritic compartments
371 from each strain were pooled across treatment groups to create a population, and the first and
372 last quartiles determined. From each branch, spines belonging to the first quartile (Q1, smallest)
373 and last quartile (Q4, largest) were identified and the density for each quartile per branch was
374 calculated. Data were analyzed with each dendrite representing an individual data point.
375
376 **Statistical analysis**
377 Data were analyzed blinded to strain and age group. All statistical analyses were performed in
378 GraphPad Prism software (v9.5.1) except for Kolmogorov-Smirnov tests which were performed
379 using R (v4.2.2). Results are reported in table form in the Supplemental Information **Table S2-**
380 **S5**). Data from B6 and PWK mouse strains were analyzed separately. To assess age effects
381 within each strain, one-way ANOVAs were computed followed by Bonferroni post hoc tests.
382 Within-group differences between Q1 and Q4 densities for spine head diameter and neck length
383 were determined using nonparametric two-tailed t-tests. Bonferroni corrections for multiple
384 comparisons were performed on nominal p-values from resultant K-S tests.
385
386 **Data and resource sharing plan**
387 All mouse strains are available through The Jackson Laboratory. All reagents in this study are
388 commercially available. Raw data (DOI: 10.6084/m9.figshare.23620752) and images from the

figures (DOI: 10.6084/m9.figshare.23620755) are available via Figshare (made public upon acceptance of publication).

Author contributions

S.E.H., E.B.B. and G.R.H. designed the study. S.E.H. generated and maintained mouse cohorts, and S.E.H. and E.B.B. performed the intracranial AAV injections. S.E.H. euthanized mice and collected tissues. S.E.H. and E.W.N. sectioned brains and prepared slides for imaging. S.E.H. and E.W.N. imaged slices and analyzed final data. E.B.B. provided training in intracranial injections, confocal microscopy imaging of dendrites and dendritic spines, and NeuronStudio analysis. E.B.B. and G.R.H. advised on all data analysis, data interpretation and manuscript preparation. S.E.H., E.W.N., E.B.B. and G.R.H. wrote and edited the manuscript. All authors approved the final version.

Competing Interest statement

The authors have no conflicts or competing interests to declare.

ACKNOWLEDGEMENTS AND FUNDING SOURCES

Acknowledgements

We thank Dr. Kristen Onos and Kelly Keezer for providing aged PWK/PhJ mouse cohorts, and Amanda Hewes and Melanie-Maddox Goodrich for providing critical laboratory support for the initiation of these experiments. We also thank Dr. Philipp Henrich at the Microscopy core at The Jackson Laboratory for training and assistance on the confocal microscope.

Funding Sources

This study was supported by the National Institute on Aging (NIA) AG079877 (E.B.B.), AG055104 (G.R.H.), program funds from The Jackson Laboratory (G.R.H.), and by the NIA T32 training

program AG062409 in the Precision Genetics of Aging, Alzheimer's Disease and Related Dementias at The Jackson Laboratory (S.E.H., G.R.H., E.B.B.).

REFERENCES

1. T. N. Lerner, L. Ye, K. Deisseroth, Communication in Neural Circuits: Tools, Opportunities, and Challenges. *Cell* **164**, 1136–1150 (2016).

2. T. C. Südhof, R. C. Malenka, Understanding Synapses: Past, Present, and Future. *Neuron* **60**, 469–476 (2008).

3. M. Sheng, E. Kim, The Postsynaptic Organization of Synapses. *Cold Spring Harb. Perspect. Biol.* **3**, a005678 (2011).

4. R. R. LLINÁS, K. D. WALTON, E. J. LANG, "Cerebellum" in *The Synaptic Organization of the Brain*, G. M. Shepherd, Ed. (Oxford University Press, 2004), p. 0.

5. I. Ballesteros-Yáñez, R. Benavides-Piccione, G. N. Elston, R. Yuste, J. DeFelipe, Density and morphology of dendritic spines in mouse neocortex. *Neuroscience* **138**, 403–409 (2006).

6. M. Matsuzaki, N. Honkura, G. C. R. Ellis-Davies, H. Kasai, Structural basis of long-term potentiation in single dendritic spines. *Nature* **429**, 761–766 (2004).

7. G. G. Turrigiano, The self-tuning neuron: synaptic scaling of excitatory synapses. *Cell* **135**, 422–435 (2008).

8. H. Kasai, M. Matsuzaki, J. Noguchi, N. Yasumatsu, H. Nakahara, Structure–stability–function relationships of dendritic spines. *Trends Neurosci.* **26**, 360–368 (2003).

9. C. D. Harvey, K. Svoboda, Locally dynamic synaptic learning rules in pyramidal neuron dendrites. *Nature* **450**, 1195–1200 (2007).

10. S. R. y Cajal, *Estructura de los centros nerviosos de las aves* (1888).

11. M. E. Serrano, E. Kim, M. M. Petrinovic, F. Turkheimer, D. Cash, Imaging Synaptic Density: The Next Holy Grail of Neuroscience? *Front. Neurosci.* **16**, 796129 (2022).

12. M. Matsuzaki, *et al.*, Dendritic spine geometry is critical for AMPA receptor expression in hippocampal CA1 pyramidal neurons. *Nat. Neurosci.* **4**, 1086–1092 (2001).

13. J. Tønnesen, G. Katona, B. Rózsa, U. V. Nägerl, Spine neck plasticity regulates compartmentalization of synapses. *Nat. Neurosci.* **17**, 678–685 (2014).

14. Å. Grunditz, N. Holbro, L. Tian, Y. Zuo, T. G. Oertner, Spine Neck Plasticity Controls Postsynaptic Calcium Signals through Electrical Compartmentalization. *J. Neurosci.* **28**, 13457–13466 (2008).

15. S. N. Burke, C. A. Barnes, Neural plasticity in the ageing brain. *Nat. Rev. Neurosci.* **7**, 30–40 (2006).

16. J. H. Morrison, M. G. Baxter, The ageing cortical synapse: hallmarks and implications for cognitive decline. *Nat. Rev. Neurosci.* **13**, 240–250 (2012).

17. D. L. Dickstein, C. M. Weaver, J. I. Luebke, P. R. Hof, Dendritic spine changes associated with normal aging. *Neuroscience* **251**, 21–32 (2013).

18. X. Fan, E. G. Wheatley, S. A. Villeda, Mechanisms of Hippocampal Aging and the Potential for Rejuvenation. *Annu. Rev. Neurosci.* **40**, 251–272 (2017).

19. M. E. Young, D. T. Ohm, D. Dumitriu, P. R. Rapp, J. H. Morrison, Differential effects of aging on dendritic spines in visual cortex and prefrontal cortex of the rhesus monkey. *Neuroscience* **274**, 33–43 (2014).

20. Y. Hara, P. R. Rapp, J. H. Morrison, Neuronal and morphological bases of cognitive decline in aged rhesus monkeys. *Age Dordr. Neth.* **34**, 1051–1073 (2012).

21. A. R. Brennan, *et al.*, Protein kinase C activity is associated with prefrontal cortical decline in aging. *Neurobiol. Aging* **30**, 782–792 (2009).

22. J. I. Luebke, Y.-M. Chang, T. L. Moore, D. L. Rosene, Normal aging results in decreased synaptic excitation and increased synaptic inhibition of layer 2/3 pyramidal cells in the monkey prefrontal cortex. *Neuroscience* **125**, 277–288 (2004).

23. S. W. Scheff, D. A. Price, D. L. Sparks, Quantitative assessment of possible age-related change in synaptic numbers in the human frontal cortex. *Neurobiol. Aging* **22**, 355–365 (2001).

24. S. W. Scheff, S. A. Scott, S. T. DeKosky, Quantitation of synaptic density in the septal nuclei of young and aged Fischer 344 rats. *Neurobiol. Aging* **12**, 3–12 (1991).

25. E. B. Bloss, *et al.*, Evidence for Reduced Experience-Dependent Dendritic Spine Plasticity in the Aging Prefrontal Cortex. *J. Neurosci.* **31**, 7831–7839 (2011).

26. M. B. Moss, T. L. Moore, S. P. Schettler, R. Killiany, D. Rosene, “Successful vs. Unsuccessful Aging in the Rhesus Monkey” in *Brain Aging: Models, Methods, and Mechanisms*, Frontiers in Neuroscience., D. R. Riddle, Ed. (CRC Press/Taylor & Francis, 2007) (June 27, 2023).

27. J. H. Morrison, P. R. Hof, Life and death of neurons in the aging brain. *Science* **278**, 412–419 (1997).

477 28. P. R. Hof, J. H. Morrison, The aging brain: morphomolecular senescence of cortical circuits.
478 *Trends Neurosci.* **27**, 607–613 (2004).

479 29. A. PETERS, C. SETHARES, J. I. LUEBKE, SYNAPSES ARE LOST DURING AGING IN THE PRIMATE
480 PREFRONTAL CORTEX. *Neuroscience* **152**, 970–981 (2008).

481 30. E. B. Bloss, *et al.*, Morphological and molecular changes in aging rat prelimbic prefrontal
482 cortical synapses. *Neurobiol. Aging* **34**, 200–210 (2013).

483 31. C. A. Barnes, B. L. McNaughton, An age comparison of the rates of acquisition and
484 forgetting of spatial information in relation to long-term enhancement of hippocampal
485 synapses. *Behav. Neurosci.* **99**, 1040–1048 (1985).

486 32. M. Cizeron, *et al.*, A brainwide atlas of synapses across the mouse life span. *Science* **369**,
487 270–275 (2020).

488 33. D. Dumitriu, *et al.*, Selective Changes in Thin Spine Density and Morphology in Monkey
489 Prefrontal Cortex Correlate with Aging-Related Cognitive Impairment. *J. Neurosci.* **30**,
490 7507–7515 (2010).

491 34. T. Rasmussen, T. Schliemann, J. C. Sørensen, J. Zimmer, M. J. West, Memory impaired aged
492 rats: no loss of principal hippocampal and subicular neurons. *Neurobiol. Aging* **17**, 143–
493 147 (1996).

494 35. A. R. Ouellette, *et al.*, Cross-Species Analyses Identify Dlgap2 as a Regulator of Age-Related
495 Cognitive Decline and Alzheimer's Dementia. *Cell Rep.* **32**, 108091 (2020).

496 36. C. L. Ackert-Bicknell, *et al.*, Aging Research Using Mouse Models. *Curr. Protoc. Mouse Biol.*
497 **5**, 95–133 (2015).

498 37. T. M. Keane, *et al.*, Mouse genomic variation and its effect on phenotypes and gene
499 regulation. *Nature* **477**, 289–294 (2011).

500 38. K. D. Onos, *et al.*, Enhancing face validity of mouse models of Alzheimer's disease with
501 natural genetic variation. *PLoS Genet.* **15**, e1008155 (2019).

502 39. C. Fernandes, *et al.*, Behavioral Characterization of Wild Derived Male Mice (Mus musculus
503 musculus) of the PWD/Ph Inbred Strain: High Exploration Compared to C57BL/6J. *Behav.*
504 *Genet.* **34**, 621–630 (2004).

505 40. S. E. Heuer, *et al.*, Genetic context controls early microglia-synaptic interactions in mouse
506 models of Alzheimer's disease. 2023.04.28.538728 (2023).

507 41. S. Gregorová, J. Forejt, PWD/Ph and PWK/Ph inbred mouse strains of Mus m. musculus
508 subspecies--a valuable resource of phenotypic variations and genomic polymorphisms.
509 *Folia Biol. (Praha)* **46**, 31–41 (2000).

510 42. D. G. R. Tervo, *et al.*, A Designer AAV Variant Permits Efficient Retrograde Access to
511 Projection Neurons. *Neuron* **92**, 372–382 (2016).

512 43. K. Graham, N. Spruston, E. B. Bloss, Hippocampal and thalamic afferents form distinct
513 synaptic microcircuits in the mouse infralimbic frontal cortex. *Cell Rep.* **37**, 109837 (2021).

514 44. H. T. Ito, S.-J. Zhang, M. P. Witter, E. I. Moser, M.-B. Moser, A prefrontal-thalamo-
515 hippocampal circuit for goal-directed spatial navigation. *Nature* **522**, 50–55 (2015).

516 45. E. W. Buss, *et al.*, Cognitive aging is associated with redistribution of synaptic weights in
517 the hippocampus. *Proc. Natl. Acad. Sci.* **118**, e1921481118 (2021).

518 46. D. A. Nicholson, R. Yoshida, R. W. Berry, M. Gallagher, Y. Geinisman, Reduction in size of
519 perforated postsynaptic densities in hippocampal axospinous synapses and age-related
520 spatial learning impairments. *J. Neurosci. Off. J. Soc. Neurosci.* **24**, 7648–7653 (2004).

521 47. Y. Geinisman, *et al.*, Aging, spatial learning, and total synapse number in the rat CA1
522 stratum radiatum. *Neurobiol. Aging* **25**, 407–416 (2004).

523 48. M. Megías, Z. Emri, T. F. Freund, A. I. Gulyás, Total number and distribution of inhibitory
524 and excitatory synapses on hippocampal CA1 pyramidal cells. *Neuroscience* **102**, 527–540
525 (2001).

526 49. E. B. Bloss, *et al.*, Single excitatory axons form clustered synapses onto CA1 pyramidal cell
527 dendrites. *Nat. Neurosci.* **21**, 353–363 (2018).

528 50. R. M. Empson, U. Heinemann, The perforant path projection to hippocampal area CA1 in
529 the rat hippocampal-entorhinal cortex combined slice. *J. Physiol.* **484**, 707–720 (1995).

530 51. T. A. Blanpied, M. D. Ehlers, Microanatomy of dendritic spines: emerging principles of
531 synaptic pathology in psychiatric and neurological disease. *Biol. Psychiatry* **55**, 1121–1127
532 (2004).

533 52. K. Runge, C. Cardoso, A. de Chevigny, Dendritic Spine Plasticity: Function and Mechanisms.
534 *Front. Synaptic Neurosci.* **12** (2020).

535 53. G. Turrigiano, Homeostatic synaptic plasticity: local and global mechanisms for stabilizing
536 neuronal function. *Cold Spring Harb. Perspect. Biol.* **4**, a005736 (2012).

537 54. R. Araya, J. Jiang, K. B. Eisenthal, R. Yuste, The spine neck filters membrane potentials.
538 *Proc. Natl. Acad. Sci.* **103**, 17961–17966 (2006).

539 55. K. E. Sorra, K. M. Harris, Overview on the structure, composition, function, development,
540 and plasticity of hippocampal dendritic spines. *Hippocampus* **10**, 501–511 (2000).

541 56. M. Wang, *et al.*, Alpha2A-adrenoceptors strengthen working memory networks by
542 inhibiting cAMP-HCN channel signaling in prefrontal cortex. *Cell* **129**, 397–410 (2007).

543 57. K. M. Neuman, *et al.*, Evidence for Alzheimer's disease-linked synapse loss and
544 compensation in mouse and human hippocampal CA1 pyramidal neurons. *Brain Struct.*
545 *Funct.* **220**, 3143–3165 (2015).

546 58. S. K. Kaufman, K. Del Tredici, T. L. Thomas, H. Braak, M. I. Diamond, Tau seeding activity
547 begins in the transentorhinal/entorhinal regions and anticipates phospho-tau pathology in
548 Alzheimer's disease and PART. *Acta Neuropathol. (Berl.)* **136**, 57–67 (2018).

549 59. H. Hampel, *et al.*, The Amyloid-β Pathway in Alzheimer's Disease. *Mol. Psychiatry* **26**,
550 5481–5503 (2021).

551 60. Z. Petanjek, *et al.*, Extraordinary neoteny of synaptic spines in the human prefrontal
552 cortex. *Proc. Natl. Acad. Sci.* **108**, 13281–13286 (2011).

553 61. S. A. Villeda, *et al.*, Young blood reverses age-related impairments in cognitive function
554 and synaptic plasticity in mice. *Nat. Med.* **20**, 659–663 (2014).

555 62. J. Hao, *et al.*, Interactive effects of age and estrogen on cognition and pyramidal neurons
556 in monkey prefrontal cortex. *Proc. Natl. Acad. Sci. U. S. A.* **104**, 11465–11470 (2007).

557 63. H. Bayer, L. J. Bertoglio, Infralimbic cortex controls fear memory generalization and
558 susceptibility to extinction during consolidation. *Sci. Rep.* **10**, 15827 (2020).

559 64. C. C. Kaczorowski, S. J. Davis, J. R. Moyer, Aging redistributes medial prefrontal neuronal
560 excitability and impedes extinction of trace fear conditioning. *Neurobiol. Aging* **33**, 1744–
561 1757 (2012).

562 65. J. L. Bizon, *et al.*, Spatial reference and working memory across the lifespan of male Fischer
563 344 rats. *Neurobiol. Aging* **30**, 646–655 (2009).

564 66. A. Shimada, H. Keino, M. Satoh, M. Kishikawa, M. Hosokawa, Age-related loss of synapses
565 in the frontal cortex of SAMP10 mouse: A model of cerebral degeneration. *Synapse* **48**,
566 198–204 (2003).

567 67. N. Spruston, Pyramidal neurons: dendritic structure and synaptic integration. *Nat. Rev.*
568 *Neurosci.* **9**, 206–221 (2008).

569 68. T. Branco, M. Häusser, Synaptic integration gradients in single cortical pyramidal cell
570 dendrites. *Neuron* **69**, 885–892 (2011).

571 69. J. C. Magee, Dendritic integration of excitatory synaptic input. *Nat. Rev. Neurosci.* **1**, 181–
572 190 (2000).

573 70. M. E. Larkum, T. Nevian, M. Sandler, A. Polsky, J. Schiller, Synaptic integration in tuft
574 dendrites of layer 5 pyramidal neurons: a new unifying principle. *Science* **325**, 756–760
575 (2009).

576 71. H. S. Yang, *et al.*, Natural genetic variation determines microglia heterogeneity in wild-
577 derived mouse models of Alzheimer's disease. *Cell Rep.* **34** (2021).

578 72. C. Pliatsikas, *et al.*, Working memory in older adults declines with age, but is modulated by
579 sex and education. *Q. J. Exp. Psychol. 2006* **72**, 1308–1327 (2019).

580 73. T. L. Moore, R. J. Killiany, J. G. Herndon, D. L. Rosene, M. B. Moss, Executive system
581 dysfunction occurs as early as middle-age in the rhesus monkey. *Neurobiol. Aging* **27**,
582 1484–1493 (2006).

583 74. T. A. Salthouse, When does age-related cognitive decline begin? *Neurobiol. Aging* **30**, 507–
584 514 (2009).

585 75. L. J. Launer, *et al.*, Rates and risk factors for dementia and Alzheimer's disease: results
586 from EURODEM pooled analyses. EURODEM Incidence Research Group and Work Groups.
587 European Studies of Dementia. *Neurology* **52**, 78–84 (1999).

588 76. R. A Armstrong, Risk factors for Alzheimer's disease. *Folia Neuropathol.* **57**, 87–105 (2019).

589 77. W. Göbel, F. Helmchen, In Vivo Calcium Imaging of Neural Network Function. *Physiology*
590 **22**, 358–365 (2007).

591 78. J. Winnubst, *et al.*, Reconstruction of 1,000 Projection Neurons Reveals New Cell Types
592 and Organization of Long-Range Connectivity in the Mouse Brain. *Cell* **179**, 268-281.e13
593 (2019).

594 79. A. Rodriguez, D. B. Ehlenberger, D. L. Dickstein, P. R. Hof, S. L. Wearne, Automated Three-
595 Dimensional Detection and Shape Classification of Dendritic Spines from Fluorescence
596 Microscopy Images. *PLoS ONE* **3**, e1997 (2008).

597 80. W. R. Holmes, The role of dendritic diameters in maximizing the effectiveness of synaptic
598 inputs. *Brain Res.* **478**, 127–137 (1989).

599

600

601

602

603

604 **MAIN FIGURES**

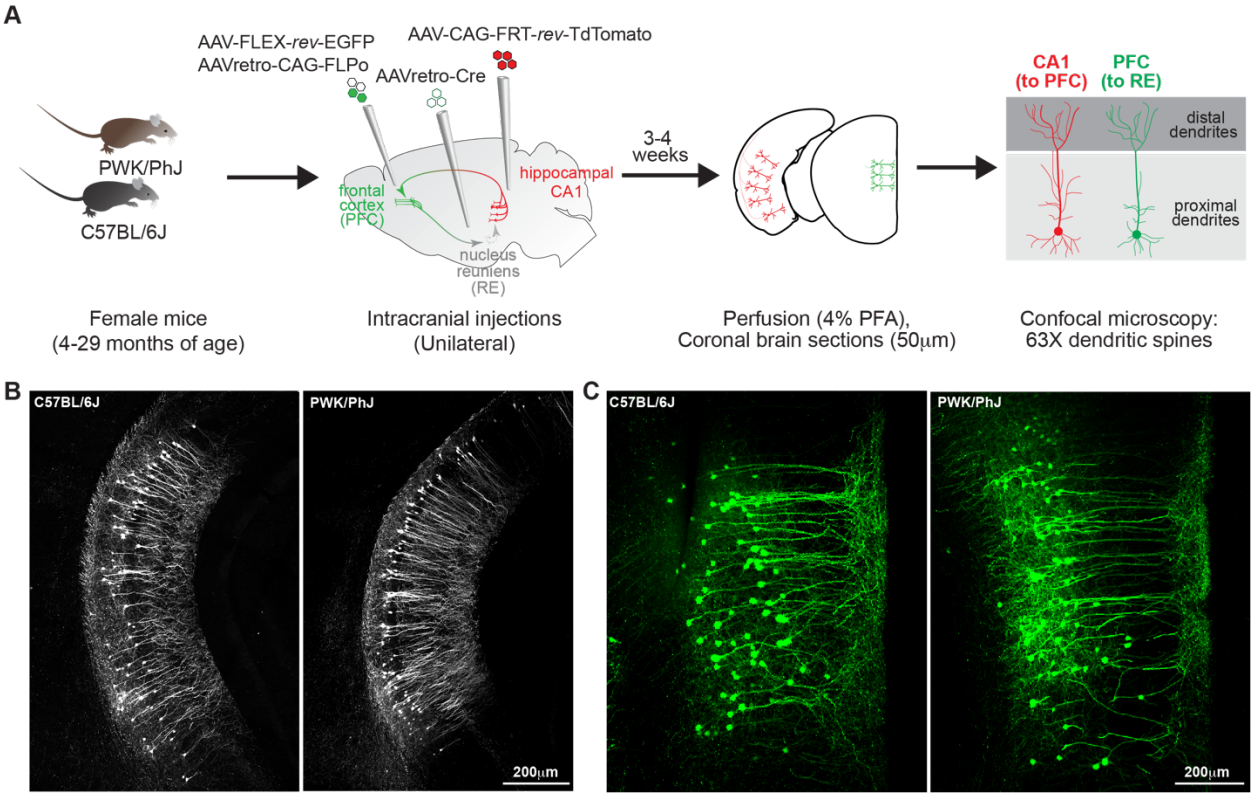

605

606 **Figure 1: Viral labeling of PFC-to-RE and CA1-to-PFC neurons across C57BL/6J and**

607 **PWK/PhJ mice.**

608 **(A)** Experimental outline (see ***Methods*** for additional details)

609 **(B-C)** Example 10X images of tdTomato+ CA1 neurons (B) from B6 (left) and PWK (right)

610 demonstrating consistent CA1-to-PFC projection circuit labeling, and EGFP+ PFC neurons (C)

611 from B6 (left) and PWK (right) demonstrating consistent PFC-to-RE projection circuit labeling.

612 Summary metadata for individual mice used in this study reported in **Table S1**.

613

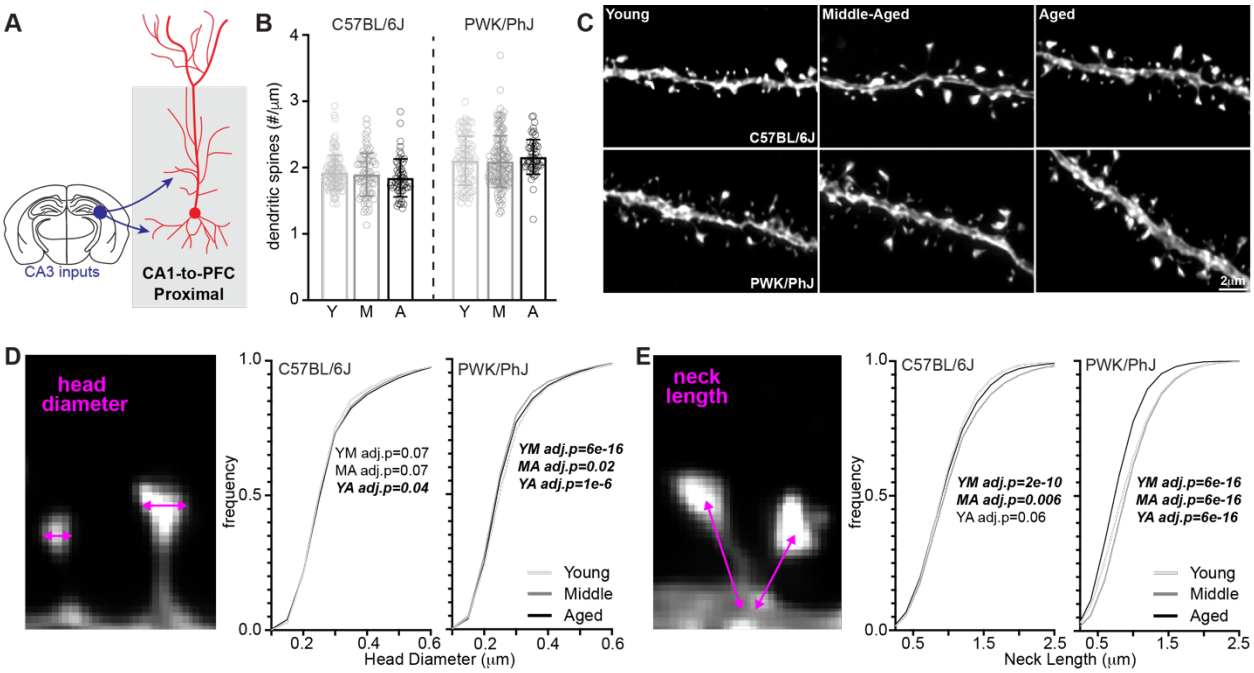

Figure 2: CA1-to-PFC proximal dendrites are resistant to synaptic density changes across both strains, but PWK/PhJ spines change morphologies.

(A) Example schematic of tdTomato+ proximal CA1-to-PFC dendrites analyzed here and projection input origins in hippocampal area CA3.

(B) Proximal CA1-to-PFC dendrite spine densities (spines/μm) comparing young (Y), middle (M) and aged (A) within each strain. Data points represent individual branches (n=20/mouse); error bars are ± SD; one-way ANOVA identified no significant effects within B6 or PWK (**Table S2**).

(C) Representative 63X images of proximal CA1-to-PFC dendrites from each strain/age group.

(D) CA1-to-PFC proximal spine head diameter example image (left) and cumulative distributions from B6 (middle) and PWK (right), across age groups. Kolmogorov-Smirnov tests were used to evaluate statistical significance (Bonferroni adj. $p<0.05$) of pairwise comparisons: young vs middle (YM), middle vs aged (MA), and young vs. aged (YA), and p-values reported on each graph (see **Table S2**). Data points are representative of measures from individual spines.

(E) Same as **(D)** for CA1-to-PFC proximal spine neck length.

Summary statistics for data points represented in each graph reported in **Table S2.**

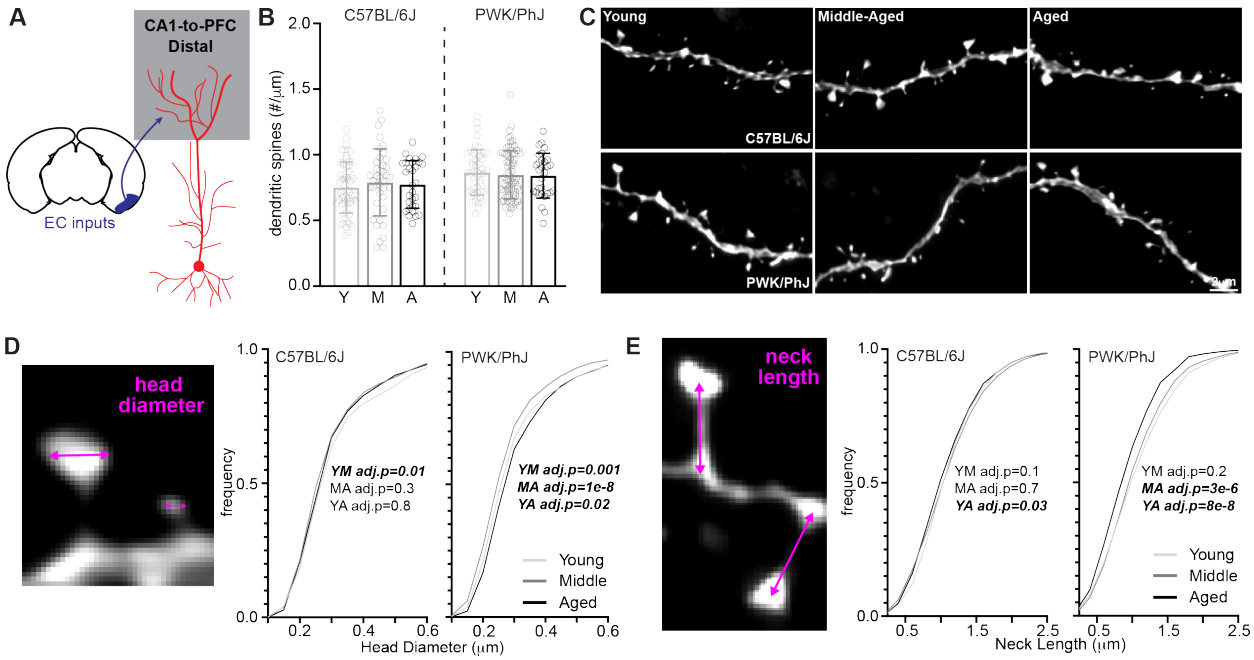

Figure 3: CA1-to-PFC distal tuft dendrites do not lose synapses but are morphologically altered in PWK/PhJ mice.

(A) Example schematic of tdTomato+ distal tuft CA1-to-PFC dendrites analyzed here and projection input origins in entorhinal cortex (EC).

(B) Distal tuft CA1-to-PFC dendrite spine densities (spines/μm) comparing young (Y), middle (M) and aged (A) within each strain. Data points represent individual branches (n=10/mouse); error bars are ± SD; one-way ANOVA identified no significant effects within B6 or PWK (**Table S3**).

(C) Representative 63X images of distal tuft CA1-to-PFC dendrites from each strain/age group.

(D) CA1-to-PFC distal tuft spine head diameter example image (left) and cumulative distributions from B6 (middle) and PWK (right), across age groups. Kolmogorov-Smirnov tests were used to evaluate statistical significance (Bonferroni adj. $p<0.05$) of pairwise comparisons: young vs middle (YM), middle vs aged (MA), and young vs. aged (YA), and p-values reported on each graph (see **Table S3**). Data points are representative of measures from individual spines.

(E) Same as **(D)** for CA1-to-PFC distal tuft spine neck length.

Summary statistics for data points represented in each graph reported in **Table S3.**

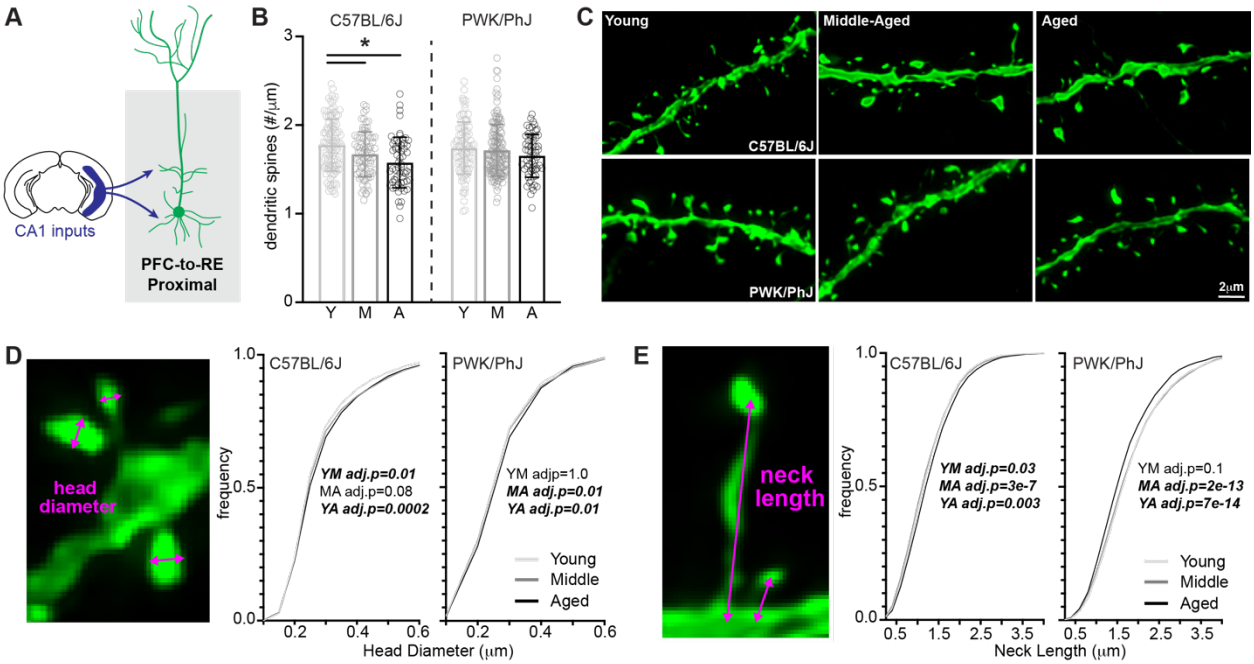

Figure 4: C57BL/6J mice are susceptible to age-related synaptic loss in proximal PFC-to-RE dendrites, with PWK/PhJ demonstrating dynamic morphological changes to increase synaptic strength.

(A) Example schematic of EGFP+ proximal PFC-to-RE dendrites analyzed here and projection input origins in hippocampal area CA1.

(B) Proximal PFC-to-RE dendrite spine densities (spines/μm) comparing young (Y), middle-aged (M) and aged (A) within each strain. Data points represent individual branches (n=20/mouse); error bars are ± SD; one-way ANOVA identified significant effect within B6 but not PWK; asterisks denote significant (Bonferroni adjusted $p<0.05$) comparisons identified using post-hoc analysis within B6 (**Table S4**).

(C) Representative 63X images of proximal PFC-to-RE dendrites from each strain/age group.

(D) PFC-to-RE proximal spine head diameter example image (left) and cumulative distributions from B6 (middle) and PWK (right), across age groups. Kolmogorov-Smirnov tests were used to evaluate statistical significance (Bonferroni adj. $p<0.05$) of pairwise comparisons: young vs middle

(YM), middle vs aged (MA), and young vs. aged (YA), and p-values reported on each graph (see **Table S4**). Data points are representative of measures from individual spines.

(E) Same as **(D)** for PFC-to-RE proximal spine neck length.

Summary statistics for data points represented in each graph reported in **Table S4.**

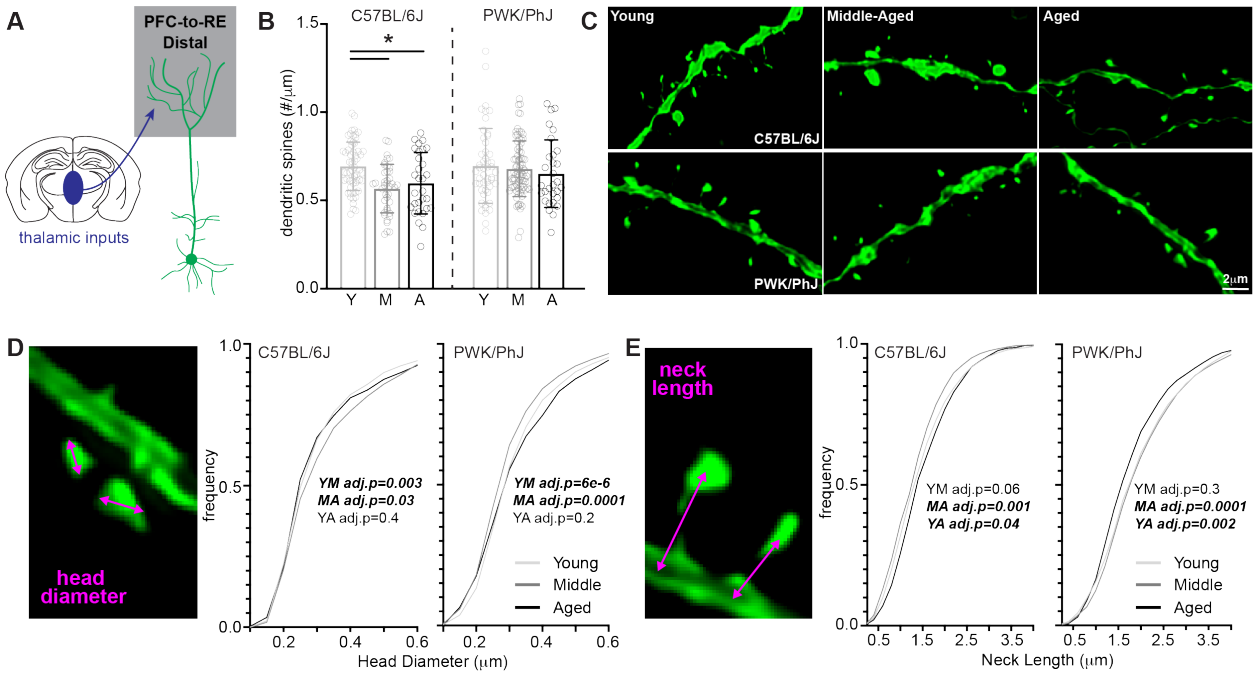

Figure 5: PFC-to-RE distal tuft dendrites exhibit age-induced synaptic loss in C57BL/6J mice but are morphology dynamic in PWK/PhJ mice.

(A) Example schematic of EGFP+ distal tuft PFC-to-RE dendrites analyzed here and thalamic projection input origins.

(B) Distal tuft PFC-to-RE dendrite spine densities (spines/μm) comparing young (Y), middle (M) and aged (A) within each strain. Data points represent individual branches (n=10/mouse); error bars are ± SD; one-way ANOVA identified significant effect within B6 but not PWK; asterisks

676 denote significant (Bonferroni adjusted $p<0.05$) comparisons identified using post-hoc analysis
677 within B6 (**Table S5**).
678 **(C)** Representative 63X images of distal tuft PFC-to-RE dendrites from each strain/age group.
679 **(D)** PFC-to-RE distal tuft spine head diameter example image (left) and cumulative distributions
680 from B6 (middle) and PWK (right), across age groups. Kolmogorov-Smirnov tests were used to
681 evaluate statistical significance (Bonferroni adj. $p<0.05$) of pairwise comparisons: young vs middle
682 (YM), middle vs aged (MA), and young vs. aged (YA), and p-values reported on each graph (see
683 **Table S5**). Data points are representative of measures from individual spines.
684 **(E)** Same as **(D)** for PFC-to-RE distal tuft spine neck length.
685 Summary statistics for data points represented in each graph reported in **Table S5.**